Non-covalent Immobilization of Iron-triazole (Fe(Htrz) 3) Molecular Mediator in Mesoporous Silica Films for the Electrochemical Detection of Hydrogen Peroxide

Samuel Ahoulou, Neus Vilà, Sébastien Pillet, Dominik Schaniel, Alain Walcarius

Non-covalent immobilization of iron-triazole ($Fe(Htrz)_3$) molecular mediator in mesoporous silica films for the electrochemical detection of hydrogen peroxide

Samuel AHOULOU,[a,b] *Neus VILA,*[a]* *Sébastien PILLET,*[b] *Dominik SCHANIEL,*[b] *Alain WALCARIUS*[a]*

[a] Laboratoire de Chimie Physique et Microbiologie pour les Matériaux et l'Environnement (LCPME), UMR7564 CNRS – Université de Lorraine, 405 rue de Vandoeuvre, 54600 Villers-les-Nancy, France
[b] Université de Lorraine, CNRS, CRM2 UMR7036, 54000 Nancy, France
* e-mail: alain.walcarius@univ-lorraine.fr, neus.vila@univ-lorraine.fr

Abstract
Mesoporous silica thin films encapsulating a molecular iron-triazole complex, $Fe(Htrz)_3$ (Htrz = 1,2,4,-1*H*-triazole), have been generated by electrochemically assisted self-assembly (EASA) on indium-tin oxide (ITO) electrode. The obtained modified electrodes are characterized by well-defined voltammetric signals corresponding to the $Fe^{II/III}$ centers of the $Fe(Htrz)_3$ species immobilized into the films, indicating fast electron transfer processes and stable operational stability. This is due to the presence of a high density of redox probes in the material (1.6×10^{-4} mol g^{-1} $Fe(Htrz)_3$ in the mesoporous silica film) enabling efficient charge transport by electron hopping. The mesoporous films are uniformly deposited over the whole electrode surface and they are characterized by a thickness of 110 nm and a wormlike mesostructure directed by the template role played by $Fe(Htrz)_3$ species in the EASA process. These species are durably immobilized in the material (they are not removed by solvent extraction). The composite mesoporous material (denoted $Fe(Htrz)_3@SiO_2$) is then used for the electrocatalytic detection of hydrogen peroxide, which can be performed by amperometry at an applied potential of -0.4 V versus Ag/AgCl and by flow injection analysis. The organic-inorganic hybrid film electrode displays good sensitivity for H_2O_2 sensing over a dynamic range from 5 to 300 µM, with a detection limit estimated at 2 µM.

Keywords: Mesoporous silica, Thin film, Iron-triazole complex ($Fe(Htrz)_3$), electrocatalytic detection, hydrogen peroxide

1. Introduction

Iron-based complexes have been the focus of great interest due to their attractiveness for applications in various fields, including catalysis, organic synthesis, optics and electronics, photo- and electrochemistry, or biology and (nano)medicine [1-7]. Among them, the iron-triazole complexes (formed upon reaction of Fe(II) with triazole ligands to give coordination polymers in solution) have received considerable attention notably for their optical, magnetic, and electronic characteristics [8-10] However, most of the metal-based catalysts may suffer from poisoning under the reaction conditions, resulting in their deactivation and loss of catalytic activity. Preparation of supported metal complexes could effectively solve this problem, which might be achieved via their dispersion in porous materials such as metal oxides, carbon or polymers. In particular, mesoporous matrices are an auspicious type of material as their porous structures with large, regular, and accessible channels make them potential candidates to act as a hosting support for several active chemical species [11-13]. For instance, mesoporous silica-based matrices have been exploited to accommodate Fe(II)-triazole complexes in the form of monolith or thin film nanocomposites [14-16]. To date, however, the electrochemical applications of such complexes remain limited in spite of their known electroactivity in solution [17].

On the other hand, ordered mesoporous silica materials coated on electrode surfaces are increasingly used for electrochemical sensing and biosensing purposes [18-20]. Of special interest are thin films offering pores accessible from the surface because they ensure fast mass transport of target species from the solution to the electrode surface, and consequently large voltammetric responses [21,22]. They can be prepared by evaporation-induced self-assembly [21,23] or by electrochemically-assisted self-assembly [24,25], this latter method enabling the generation of vertically oriented mesopore channels which are particularly suited to analytical applications [20,26]. Some attempts have been already made to immobilize redox mediators within mesoporous silica thin films on electrodes. A straightforward approach is the simple doping using redox-active species that are likely to interact with the silica surface via weak bonds (electrostatic interactions), as reported for $[Ru(bpy)_3]^{2+}$ [27,28], but such weakly bound species can leach out of the film, resulting in rather poor operational stability in multisweep cyclic voltammetry, for instance [27]. More durable immobilization is achieved by covalent binding of the redox moieties onto [29-32] or into [33] the mesopore

walls, but such groups physically attached to an insulating material as silica can be electrochemically accessible only via electron hopping between adjacent sites, resulting in effective charge propagation through the film in case of redox centers very close to each other (i.e., high content) [29,34]. Long-range charge transfer by electron hopping has been demonstrated for a vertically-aligned ferrocene-functionalized film [35], but the rate of charge transfer remains limited [34], except in special configuration [36]. Promising ways to promote charge transport in mesoporous silica films are via conducting polymers electropolymerized in the mesopore channels [37] or via the use of redox-active coordination polymers as template in the synthesis of the films [38] because these strategies ensure the electroactive moieties being very close to each other in the hybrid film. Here, we plan to use the iron-triazole complex, $Fe(Htrz)_3$ (Htrz = 1,2,4,-1*H*-triazole), as coordination polymer template to generate $Fe(Htrz)_3$-doped mesoporous silica films by electrochemically-assisted self-assembly (EASA) on indium-tin oxide (ITO) electrode and its subsequent use for the electrocatalytic detection of hydrogen peroxide.

Detection of hydrogen peroxide is relevant to various domains (biological, pharmaceutical, medical and environmental fields, or food and textile industry), and electrochemical methods have been developed for that purpose [39]. They include protein-based electrochemical biosensors [40,41] and nonenzymatic sensors involving the use of either charge transfer mediators [42,43] or nanomaterials [44-46], or a combination of both [47,48], or even nanocomposites (such as Pt nanoparticles and polyaniline hosted in mesoporous silica film [49]), in order to lower the high overpotentials usually associated to the electrochemical transformation of H_2O_2. Widely used mediators for H_2O_2 sensing are Prussian Blue and related derivatives [50] as well as organic or organometallic compounds [42], often deposited onto electrode surfaces as polymeric coatings or as covalently attached moieties [43,51]. Free molecular organic redox mediators are much less used because the resulting devices may suffer from poor long-term stability. Here we would like to exploit the durable immobilization of $Fe(Htrz)_3$ complexes simply entrapped in a mesoporous silica film in the course of its generation by EASA on ITO electrodes to investigate their potential interest in electrocatalysis, using hydrogen peroxide as model analyte. After a brief physico-chemical characterization of the films, in order to point out the successful deposition of the mesoporous hybrid material encapsulating $Fe(Htrz)_3$ species in an electroactive form, the modified electrode will be applied to H_2O_2 sensing by amperometry and flow injection analysis.

2. Experimental

2.1. Chemicals

Most chemicals and reagents were commercially available and used as received: tetraethoxysilane (TEOS, 98%, Alfa Aesar), cetyltrimethylammonium bromide (CTAB, 99%, Acros), ethanol (95-96%, Merck), HCl (37% Riedel de Haen), $NaNO_3$ (99%, Fluka), H_2O_2 (30%, WWR Chemicals) and ferrocene dimethanol (FcMeOH, analytical grade, Alfa Aesar). The $Fe(Htrz)_3$ coordination polymer was prepared as previously described [14], from the reaction between $Fe(BF_4)_2$ and 1,2,4,1*H*-triazole.

2.2. Electrode preparation

Indium-tin oxide (ITO) plates (surface resistivity 8-12 Ω, from Delta Technologies) or fluorine-doped tin oxide (FTO) plates (surface resistivity 7 Ω, from Solaronix) were used as supports for film growth. $Fe(Htrz)_3$-containing mesoporous silica films were generated by adapting the previously reported EASA method [24,25]. A sol solution was first prepared by adding TEOS (100 mM), CTAB (32 mM) and the $Fe(Htrz)_3$ complex (5 mM, optimized value [38]) to a 50:50 water:ethanol medium containing also 0.1 M $NaNO_3$ as electrolyte. Its pH was adjusted to 3 by adding 0.1 M HCl and the sol was aged for 2.5h to ensure proper hydrolysis of the silica precursors. It was then transferred to the electrochemical cell mounted with an ITO plate at the bottom and the electrode potential was biased at a cathodic value of -1.3 V for 20 s (optimized parameters [25]) to initiate the self-assembly condensation process and concomitant growth of the mesoporous $Fe(Htrz)_3$-silica hybrid coating ($Fe(Htrz)_3@SiO_2$). The electrode was then removed and thoroughly rinsed with water. It was aged overnight at 130°C to stabilize the obtained mesostructure. The films were washed with an ethanol solution containing 0.1 M HCl in order to remove traces of CTAB and unwanted silica aggregates that may have formed upon synthesis.

2.3. Apparatus

A μAutoLab III potentiostat (Eco Chemie, monitored by the GPES software) was used for all the electrochemical experiments, i.e., the film synthesis, its voltammetric characterization and H_2O_2 detection. A home-made electrochemical cell with a conical shape and a three electrode configuration was employed for preparation of the mesoporous films. The working electrode was placed at the bottom, the stainless steel counter electrode took place on the cell walls and an AgCl-coated silver wire served as pseudo-reference electrode. The setup was slightly modified for the electrochemical characterization of the Fe(Htrz)-functionalized films, using this time a Ag/AgCl reference electrode (Metrohm) and a platinum rod as counter electrode. Flow injection analysis (FIA) was performed in the amperometric mode (by applying a constant potential of -0.4 V unless specified otherwise), while injecting 100-μL aliquots of H_2O_2 at the desired concentration in the carrier solution (0.1 M $NaNO_3$) flowing at a rate of 1 mL min^{-1} (optimized value). The film morphology was examined by scanning electron microscopy (SEM) using the JEOL JSM-840 apparatus, and its structure was observed by transmission electron microscopy (TEM) with the aid of a ACCEL ARM 200F microscope operating at an acceleration voltage of 200 kV. Fourier transform infrared spectroscopy (FTIR) measurements were carried out by using a Nicolet 8700 apparatus equipped with a diffuse reflectance accessory (Smart Collector).

3. Results and discussions

The electrochemical behavior of the $Fe(Htrz)_3$ complex in aqueous medium is illustrated at Figure 1, showing an irreversible cyclic voltammogram with an ill-defined anodic signal around +1.0 V and a cathodic peak located at -0.25 V on scan reversal (see curve (a) in Fig. 1), which can be attributed to the $Fe^{II/III}$ redox system.

FIGURE 1

In the presence of H_2O_2, the intensity of the cathodic peak is increased (see curve (b) in Fig. 1), indicating that the $Fe(Htrz)_3$ is indeed likely to act as a mediator for the electrocatalytic reduction of hydrogen peroxide, by decreasing the overpotential by more than 500 mV with respect to the direct reduction of H_2O_2 on ITO (compare to curve (c) in Fig. 1). This confirms the possible interest of the $Fe(Htrz)_3$ complex for electrocatalytic purpose.

3.1. Characterization of the $Fe(Htrz)_3$-containing mesoporous silica film

Figure 2 confirms the successful incorporation of the coordination polymer in the mesoporous silica film prepared by EASA in the presence of $Fe(Htrz)_3$ in the starting sol. The observed voltammetric signals are well-defined and much more reversible than for the complex in solution (i.e., easier oxidation of Fe^{II} into Fe^{III}), indicating a stabilizing effect of the silica matrix.

FIGURE 2

Indeed, the negatively-charged silica surface is likely to stabilize the $Fe(Htrz)_3$ complex via electrostatic interactions, which are thought to be at the origin of the self-assembly process (driving force for mesoporous film formation). Interestingly, the reversible signals located at -0.35 V vs. Ag/AgCl remained well-defined up to rather high potential scan rates (above 1 V s^{-1}), yet with cathodic-to-anodic peak potential differences increasing at higher speeds, and peak currents were directly proportional to the potential scan rate in the 0.1–4 V s^{-1} range (see bottom inset in Fig. 2). This indicates fast and surface-confined charge transfer reactions. Compared to the mesoporous silica films grafted with redox-active groups, which are characterized by rather slow electron transport kinetics and voltammetric responses usually controlled by diffusion (i.e., pseudo-diffusion of electrons, resulting in peak currents varying linearly with the square root of scan rate) [29,34], the present system is more efficient thanks to the very close proximity of redox sites in the coordination polymer enabling easy electron hopping. This is consistent with the high density of redox probes in the material (1.6×10^{-4} mol g^{-1} $Fe(Htrz)_3$ in the film, as estimated from the integration of peak currents in Fig. 2, giving a charge of 27 μC, corresponding to a surface concentration of 1.4×10^{-9} mol cm^{-2}, and taking into account the electrode area, 0.196 cm^2, the film diameter, 5 mm, its thickness, 110 nm, and density, 0.8 g cm^{-3} (as estimated from that of MCM-41 [52])).

Robust and durable voltammetric responses have been obtained (Fig. 3A), even at high scan rate (up to 5 V s^{-1}), before and after treatment of the electrode in ethanol/HCl (a medium usually used for surfactant template extraction from mesoporous silica films [25]), and peak currents remained constant upon multiple successive voltammetric scans (data not shown). The good stability and durable immobilization of the $Fe(Htrz)_3$ template into the film was further confirmed by permeability measurements using a redox probe in solution (ferrocene dimethanol, FcMeOH), showing the absence of any noticeable current response neither before nor after treatment in ethanol/HCl (Fig. 3B). This confirms that a crack-free film recovers well the whole ITO surface and that $Fe(Htrz)_3$ species are not removed by solvent extraction (no possibility for the FcMeOH probe to cross the film and reach the electrode surface, contrary to what happened for the same kind of films pepared by EASA using a classical surfactant template [24]). Actually, for such $Fe(Htrz)_3@SiO_2$ film, almost no CTAB is incorporated during synthesis and the coordination polymer made of $Fe(Htrz)_3$ species is playing itself the role of template which is strongly entrapped in the mesopore channels [38], explaining why the nanocomposite film is totally impermeable to external redox probes (Fig. 3B) and in that potential window the $Fe(Htrz)_3$ complex is not electrochemically accessible.

FIGURE 3

Figure 4A gathers top SEM views of the film electrode, indicating a uniform morphology, yet with some particles or aggregates on top of the materials (as common for such deposits generated by EASA [24]), which are mostly eliminated after 15 min treatment in stirred solution (HCl/ethanol). In agreement to previous observations [38], TEM micrographs indicate the existence of a quite regular wormlike mesostructured (Fig. 4B) with mesochannels having the tendency to orient vertically (see inset in Fig. 4B) although not so overwhelming as for non-functionalized mesoporous silica films [24,25]. The film thickness is 110 nm, a constant value over the whole film area. FTIR spectra (Fig. 4C) confirm the expected composition of the hybrid film, with typical signatures for silica and the the iron-triazole complex, $Fe(Htrz)_3$ (from the typical vibration bands of =C-H, -N-H, -C=N and -N=N groups [53,54]). Again, no noticeable difference can be observed before and after HCl/ethanol treatment, confirming that the iron-triazole coordination polymer acting as template is strongly embedded in the mesostructure and can be thus used as a durably-immobilized redox catalyst, as shown hereafter for the amperometric detection of H_2O_2. Further characterization (XPS, diffraction patterns) can be found in our previous work [38].

FIGURE 4

3.2. Electrocatalytic detection of H_2O_2

Cyclic voltammetry was first used to evidence the effective electrocatalytic properties of the $Fe(Htrz)_3$-based mesoporous silica film towards H_2O_2 reduction and to evaluate the most appropriate electrode support between two conductive oxides (Fig. 5). As shown, the addition of H_2O_2 in the medium leads to a noticeable increase of the cathodic signal in both cases, featuring marked electrocatalysis independently on the nature of the support ITO or FTO (fluorine-doped tin oxide). The intensity of the catalytic response is more important on FTO, but the signal is shifted towards a more cathodic value (by ca. 200 mV), as a result of larger overpotential for $Fe(Htrz)_3$ on FTO (Fig. 5A) than on ITO (Fig. 5B). ITO will be thus used in further experiments as lowering overpotentials is often a prerequisite in electrochemical sensing.

FIGURE 5

H_2O_2 detection was then performed by amperometry at constant potential by injecting aliquots of the analyte at increasing concentrations in 0.1 M $NaNO_3$ aqueous solution under constant stirring. The effect of the applied potential on the amperometric response is illustrated in Figure 6A. Too low potential values (e.g., -0.2 V) do not allow reaching steady-state currents (they are decreasing with time as a result of too small interconversion of $Fe^{II/III}$ centers). More cathodic potentials (e.g., -0.4 V) enable to reach more intense and stable current values, proportional to the concentration of H_2O_2, while more cathodic values have to be avoided for reason of too large overpotentials. The value of -0.4 V is thus chosen in further experiments. In these conditions, a linear current response is obtained for H_2O_2 in the 5-300 µM concentration range (Fig. 6B), with a sensitivity of 1.9 A mol^{-1} cm^{-2} and a detection limit estimated at 2 µM (S/N = 3). The response time is very short (only 3 s to reach >90% of the steady-state currents), thanks to the fast

electron transfer kinetics associated to the immobilized $Fe(Htrz)_3$ catalyst (Fig. 2). By comparison, no detectable response can be seen when using bare ITO biased at the same potential of -0.4 V, confirming again the electrocatalytic properties of $Fe(Htrz)_3$ species embedded into the mesoporous silica film. Good operational stability is also observed over prolonged use (hour timescale, see Fig. 6C), which agrees with the highly stable electrochemical response of a nanocomposite film bearing durably the iron-triazole complex in an active form.

FIGURE 6

In addition, the modified electrode was accommodated to an electrochemical flow cell in order to evaluate its possible use for the flow injection analysis (FIA) of H_2O_2. Typical results are illustrated on Figure 7. After optimization of the operational parameters (injected volume, solution flow rate), good repeatability can be achieved (i.e., 2.7 % standard deviation (n = 9) for the analysis of 30 µM H_2O_2, see Fig. 7A), along with a correct dynamic response upon successive analyses of increasing-decreasing concentrations (Fig. 7B), indicating the absence of memory effects. A linear calibration curve is obtained in the 5-300 µM H_2O_2 concentration range (Fig. 7C).

FIGURE 7

Finally, the feasibility of the proposed electrode for practical analysis was evaluated for the determination of H_2O_2 in a commercially available disinfectant (hydrogen peroxide, Mercurochrome, Juva Santé, Paris). After appropriate dilution (10 000 times) and measuring with the standard addition method, it gave rise to a value of 89 ± 3 µM, consistent with that obtained with using the classical potassium permanganate titration (88 ± 2 µM) [55] thus confirming the accuracy of the present electrochemical method.

4. Conclusion

In this work, we have successfully immobilized an iron-triazole complex, $Fe(Htrz)_3$, in a mesoporous silica film generated by electrochemically assisted self-assembly. The effective and durable entrapment is ensured by the template role played by such coordination polymer in the course of film deposition, owing to favorable electrostatic interactions between the cationic complex and the silica surface. The encapsulated species exhibit remarkable electrochemical features, with reversible thin-layer behavior above 1 V s^{-1}, indicating of fast electron transfer processes occurring throughout the insulating silica film. The hybrid nanocomposite film electrode can be applied to the electrocatalytic detection of hydrogen peroxide, constituting the first use of $Fe(Htrz)_3$ as redox mediator. Good sensitivity and operational stability have been achieved in both amperometry and flow injection analysis, thanks to the stable immobilization of $Fe(Htrz)_3$ in an active form into the film onto the electrode surface. When operating at an applied potential of -0.4 V, H_2O_2 sensing was possible over a dynamic concentration range from 5 to 300 µM.

5. Acknowledgements

We are grateful to the CNRS, the French PIA project "*Lorraine Université d'Excellence*" (reference ANR-15-IDEX-04-LUE), and the CPER (program *SusChemProc*), for financial supports. SA acknowledges a PhD fellow from the *Université de Lorraine*. We also thank Jaafar Ghanbaja for TEM imaging.

6. References

[1] I. Bauer H.-J. Knölker, *Chem. Rev.* **2015**, *115*, 3170-3387.

[2] G. F. Manbeck, E. Fujita, *J. Porphyr. Phthalocyanines* **2015**, *19*, 45-64.

[3] G. Bauera, X. Hu, *Inorg. Chem. Front.* **2016**, *3*, 741-765.

[4] P. Jia, R. Ouyang, P. Cao, X. Zhou, T. Lei, Y. Zhao, N. Guo, H. Chang, Y. Miao, S. Zhou, *J. Coord. Chem.* **2017**, *70*, 2175-2201.

[5] J. Chen, W. R. Browne, *Coord. Chem. Rev.* **2018**, *374*, 15-35.

[6] K. S. Kjær, N. Kaul, O. Prakash, P. Chábera, N. W. Rosemann, A. Honarfar, O. Gordivska, L. A. Fredin, K.-E. Bergquist, L. Häggström, T. Ericsson, L. Lindh, A. Yartsev, S. Styring, P. Huang, J. Uhlig, J. Bendix, D. Strand, V. Sundström, P. Persson, R. Lomoth, K. Wärnmark, *Science* **2019**, *363*, 249-253.

[7] Y. Saygili, M. Stojanovic, N. Flores-Díaz, S. M. Zakeeruddin, N. Vlachopoulos, M. Grätzel, A. Hagfeldt, *Inorganics* **2019**, *7*, 30.

[8] H. Matsukizono, K. Kuroiwa, N. Kimizuka, *J. Am. Chem. Soc*. **2008**, 130, 5622-5623.

[9] O. Roubeau, *Chem. Eur. J.* **2012**, 18, 15230-15244.

[10] I. Bräunlich, A. Sanchez-Ferrer, M. Bauer, R. Schepper, P. Knüsel, J. Dshemuchadse, R. Mezzenga, W. Caseri, *Inorg. Chem*. **2014**, 53, 3546-3557.

[11] K. Moller, T. Bein, *Chem. Mater.* **1998**, *10*, 2950-2963.

[12] A. C. Sharma, A. S. Borovik, *J. Am. Chem. Soc.* **2000**, *122*, 8946-8955.

[13] M. Sohmiya, K. Saito, M. Ogawa, *Sci. Technol. Adv. Mater.* **2015**, *16*, 054201.

[14] P. Durand, S. Pillet, E.-E. Bendeif, C. Carteret, M. Bouazaoui, H. El Hamzaoui, B. Capoen, L. Salmon, S. Hébert, J. Ghanbaja, L. Aranda, D. Schaniel, *J. Mater. Chem. C* **2013**, *1*, 1933-1942.

[15] T. Zhao, L. Cuignet, M. M. Dirtu, M. Wolff, V. Spasojevic, I. Boldog, A. Rotaru, Y. Garcia, C. Janiak, *J. Mater. Chem. C* **2015**, *3*, 7802-7812.

[16] H. Voisin, C. Aimé, A. Vallée, A. Bleuzen, M. Schmutz, G. Mosser, T. Coradin, C. Roux, *J. Mater. Chem. C* **2017**, *5*, 11542-11550.

[17] K. Kuroiwa, N. Kimizuka, *Chem. Lett.* **2010**, *39*, 790-791.

[18] A. Walcarius, *Electroanalysis* **2015**, *27*, 1303-1340.

[19] M. Etienne, L. Zhang, N. Vilà, A. Walcarius, *Electroanalysis* **2015**, *27*, 2028-2054.

[20] F. Yan, X. Lin, B. Su, *Analyst* **2016**, *141*, 3482-3495.

[21] M. Etienne, A. Quach, D. Grosso, L. Nicole, C. Sanchez, A. Walcarius, *Chem. Mater.* **2007**, *19*, 844-856.

[22] M. Etienne, Y. Guillemin, D. Grosso, A. Walcarius, *Anal. Bioanal. Chem.* **2013**, *405*, 1497-1512.

[23] D. Grosso, F. Cagnol, G. J. A. A. Soler-Illia, E. L. Crepaldi, H. Amenitsch, A. Brunet-Bruneau, A. Bourgeois, C. Sanchez, *Adv. Funct. Mater.* **2004**, *14*, 309-322

[24] A. Walcarius, E. Sibottier, M. Etienne, J. Ghanbaja, *Nature Mater.* **2007**, *6*, 602-608.

[25] A. Goux, M. Etienne, E. Aubert, C. Lecomte, J. Ghanbaja, A. Walcarius, *Chem. Mater.* **2009**, *21*, 731-741.

[26] A. Walcarius, *Curr. Opin. Electrochem.* **2018**, *10*, 88-97.

[27] C. Song, G. Villemure, *Microporous Mesoporous Mater.* **2001**, *44-45*, 679-689.

[28] Z. Zhou, W. Guo, L. Xu, Q. Wang, B. Su, *Anal. Chim. Acta* **2015**, *886*, 48-55.

[29] D. Fattakhova Rohlfing, J. Rathousky, Y. Rohlfing, O. Bartels, M. Wark, *Langmuir* **2005**, *21*, 11320-11329.

[30] O. Sel, S. Sallard, T. Brezesinski, J. Rathouský, D. R. Dunphy, A. Collord, B. M. Smarsly. *Adv. Funct. Mater.* **2007**, *17*, *3241*-3250.

[31] N. Vilà, J. Ghanbaja, E. Aubert, A. Walcarius, *Angew. Chem. Int. Ed.* **2014**, *53*, 2945-2950.

[32] N. Vilà, J. Ghanbaja, A. Walcarius, *Adv. Mater. Interfaces* **2016**, *3*, 1500440.

[33] M. Luka, S. Polarz, *J. Mater. Chem. C* **2015**, *3*, 2195-2203.

[34] N. Vilà, A. Walcarius, *Electrochim. Acta* **2015**, *179*, 304-314.

[35] N. Vilà, E. André, R. Ciganda, J. Ruiz, D. Astruc, A. Walcarius, *Chem. Mater.* **2016**, *28*, 2511-2514.

[36] P. Audebert, N. Vilà, C. Allain, F. Maisonneuve, A. Walcarius, P. Hapiot, *ChemElectroChem*, **2015**, *2*, 1695-1698.

[37] A. Gamero-Quijano, C. Karman, N. Vilà, G. Herzog, A. Walcarius, *Langmuir* **2017**, *33*, 4224-4234.

[38] S. Ahoulou, N. Vilà, S. Pillet, D. Schaniel, A. Walcarius, *Chem. Mater.* **2019**, *31*, 5796-5807.

[39] W. Chen, S. Cai, Q.-Q. Ren, W. Wen, Y.-D. Zhao, *Analyst* **2012**, *137*, 49-58.

[40] A. K. Yagati, J.-W. Choi, *Electroanalysis* **2014**, *26*, 1259-1276.

[41] Z. S. Aghamiri, M. Mohsennia, H.-A. Rafiee-Pour, *Talanta* **2018**, *176*, 195-207.

[42] P. N. Mashazi, N. Nombona, M. Muchindu, S. Vilakazi, *J. Porphyr. Phthalocyanines* **2012**, *16*, 741-753.

[43] A. S. Kumar, P. Gayathri, in *Handbook of Functional Nanomaterials*, Vol. 3 (Eds.: M. Aliofkhazraei), Nova Science Publishers, Inc., Hauppauge, N. Y., **2014**, pp. 377-392.

[44] J. Kruusma, V. Sammelselg, C. E. Banks, *Electrochem. Commun.* **2008**, *10*, 1872-1875.

[45] S. Chen, R. Yuan, Y. Chai, F. Hu, *Microchim. Acta* **2013**, *180*, 15-32.

[46] R. Zhang, W. Chen, *Biosens. Bioelectron.* **2017**, *89*, 249-268.

[47] P. C. Pandey, B. Singh, *Biosens. Bioelectron.* **2008**, *24*, 842-848.

[48] R. Ramachandran, S.-M. Chen, G. P. G. Kumar, P. Gajendran, A. Xavier, N. B. Devi, *Int. J. Electrochem. Sci.* **2016**, *11*, 1247-1270.

[49] L. Ding, B. Su, *J. Electroanal. Chem.* **2015**, *736*, 83-87.

[50] E. Y. Jomma, N. Bao, S.-N. Ding, *Curr. Anal. Chem.* **2016**, *12*, 512-522.

[51] W. Liu, H. Pan, C. Liu, C. Su, W. Liu, K. Wang, J. Jiang, *ACS Appl. Mater. Interfaces* **2019**, *11*, 11466-11473.

[52] K. J. Edler, P. A. Reynolds, P. J. Branton, F. Trouw, J. W. White, *J. Chem. Soc. Faraday Trans.* **1997**, *93*, 1667-1674.

[53] M. K. Trivedi, R. M. Tallapragada, A. Branton, D. Trivedi, G. Nayak, R. K. Mishra, S. Jana, *J. Mol. Pharm. Org. Process Res.* **2015**, *3*, 128.

[54] Z. Mokadem, S. Mekki, S. Saïdi-Besbes, G. Agusti, A. Elaissari, A. Derdour, *Arabian J. Chem.* **2017**, *10*, 1039-1051.

[55] S.-J. Li, J.-C. Zhang, J. Li, H.-Y. Yang, J.-J. Meng, B. Zhang, *Sens. Actuators B* **2018**, *260*, 1-11.

List of Figures

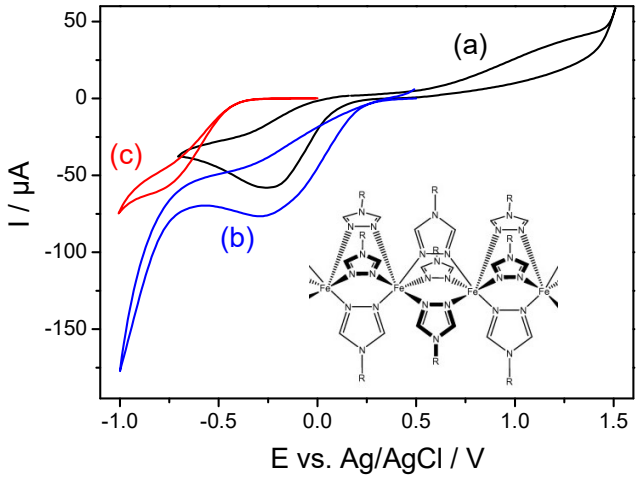

Fig. 1. Cyclic voltammograms recorded at 100 mV s^{-1} on bare ITO electrode in 0.1 M $NaNO_3$ solution (at pH 3.5) containing 5 mM $Fe(Htrz)_3$ (a) alone or (b) in the presence of 5 mM H_2O_2; (c) curve obtained for 5 mM H_2O_2 alone. Insert: $Fe(Htrz)_3$.

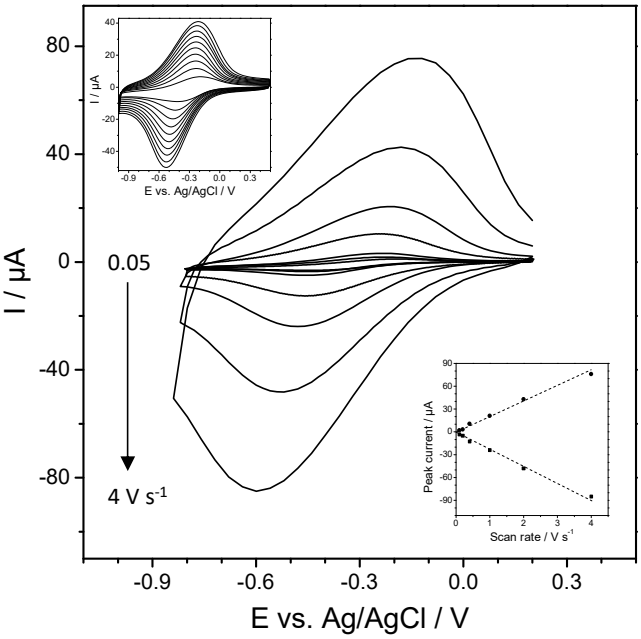

Fig. 2. Cyclic voltammograms recorded at various potential scan rates (0.05–4 V s^{-1} range and zoom on 0.1–1 V s^{-1} in top inset) in 0.1 M $NaNO_3$ solution using a mesoporous silica film bearing $Fe(Htrz)_3$ (top illustration); the variation of peak currents with potential scan rate is shown in bottom inset.

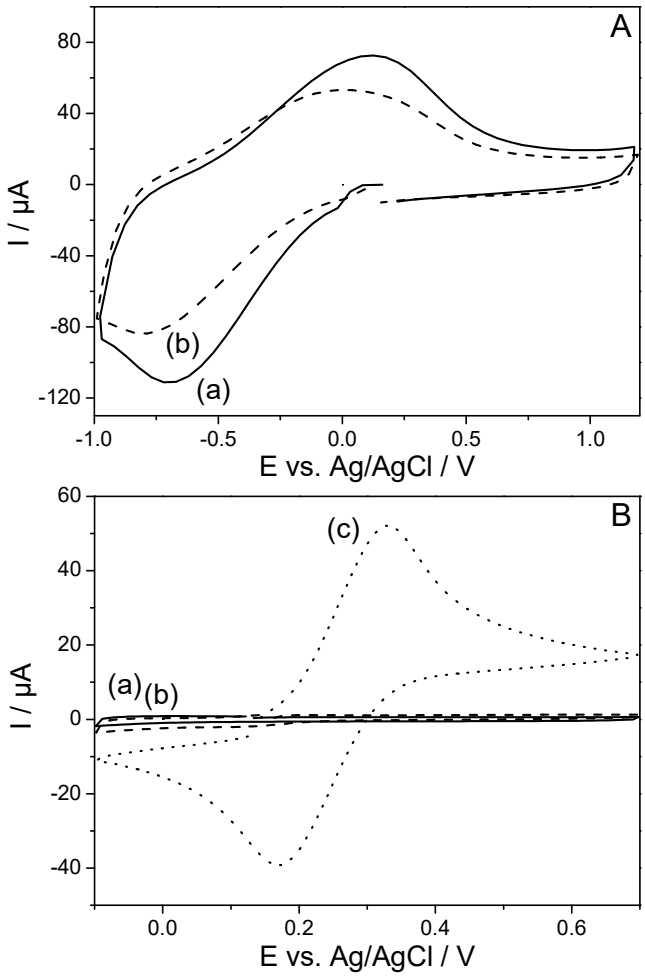

Fig. 3. (A) Cyclic voltammograms recorded at 5 V s^{-1} in 0.1 M $NaNO_3$ solution using a mesoporous silica film bearing $Fe(Htrz)_3$ (a) after or (b) before treatment in an ethanol solution containing 0.1 M HCl for 15 min. (B) Cyclic voltammograms recorded at 100 mV s^{-1} in 1 mM $Fc(MeOH)_2$ (+0.1 M $NaNO_3$) aqueous solution using the same electrode as in (A), also (a) after or (b) before treatment in HCl/ethanol; the dotted line (c) is the voltammogram recorded at bare ITO electrode.

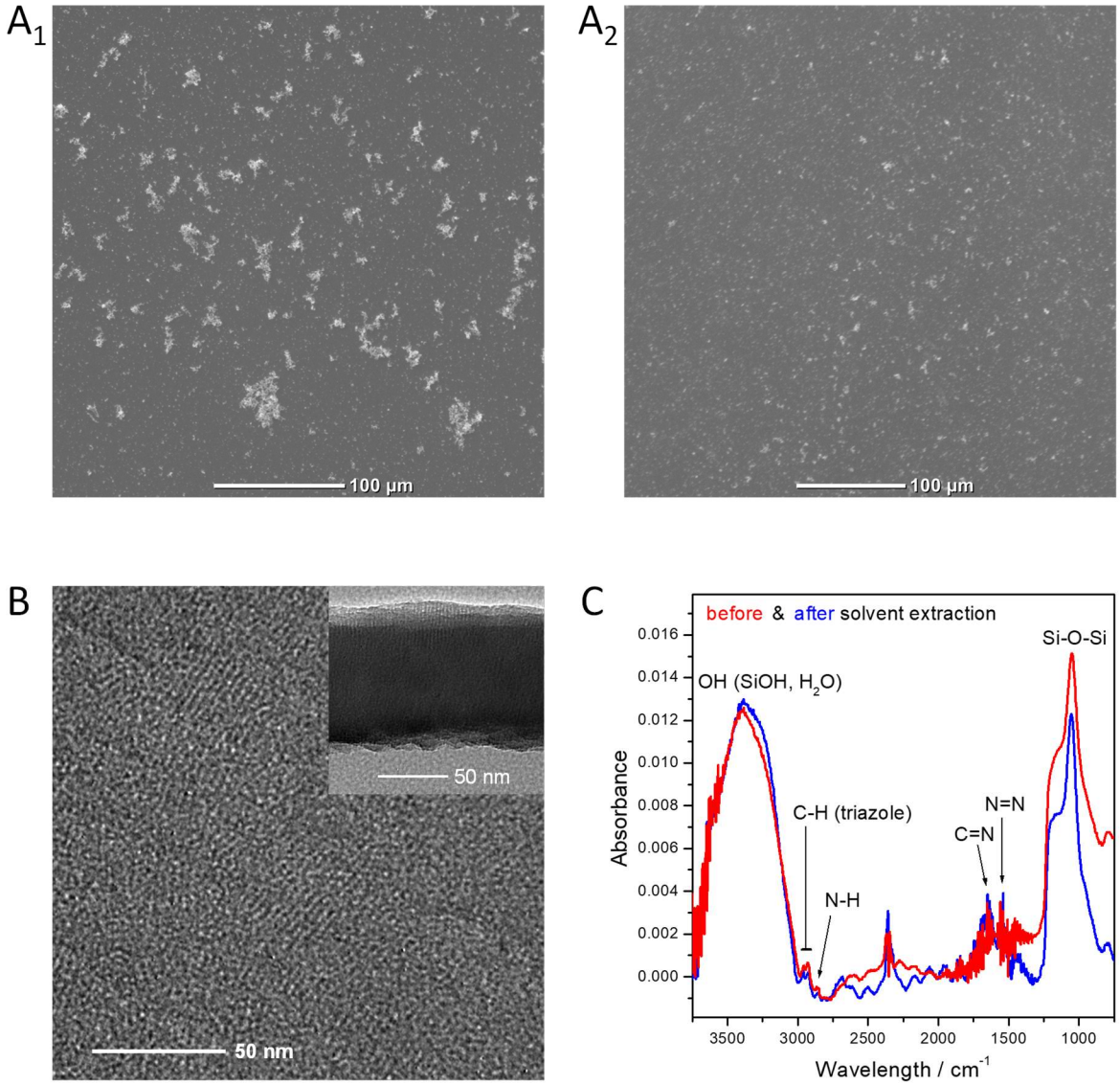

Fig. 4. (A) SEM and (B) TEM micrographs of the $Fe(Htrz)_3$-based mesoporous silica film; SEM has been respectively obtained (A_1) before and (A_2) after 15 min soaking in HCl/ethanol; TEM images in (B) correspond to top view and a cross-section as inset. (C) FTIR spectra recorded for the same film, before (red curve) and after (blue curve) HCl/ethanol treatment.

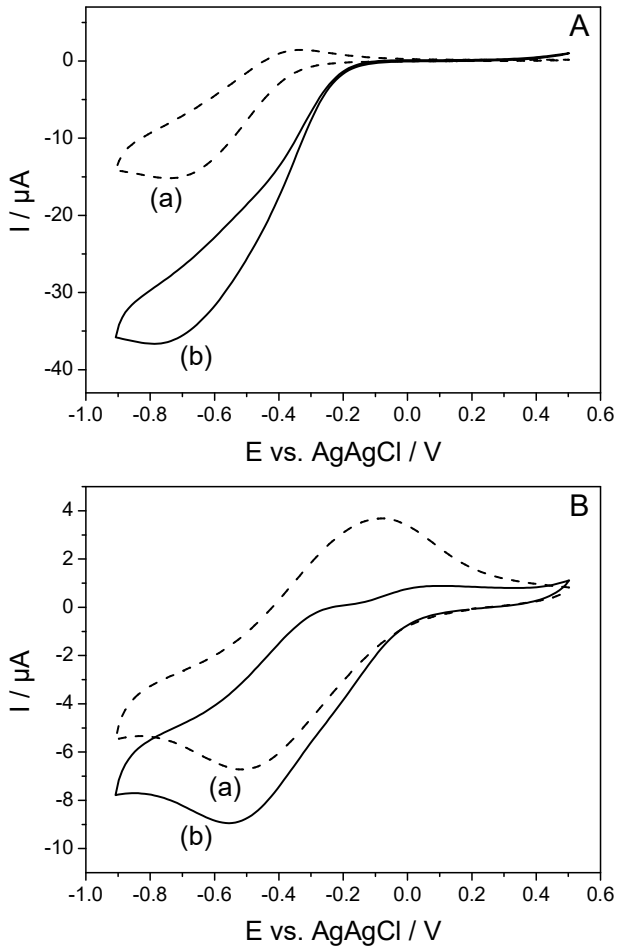

Fig. 5. Cyclic voltammograms recorded at 100 mV s^{-1} in 0.1 M $NaNO_3$ aqueous solution using (A) FTO or (B) ITO electrodes covered with a mesoporous silica film bearing $Fe(Htrz)_3$, (a) before and (b) after addition of 1 mM H_2O_2 in the medium.

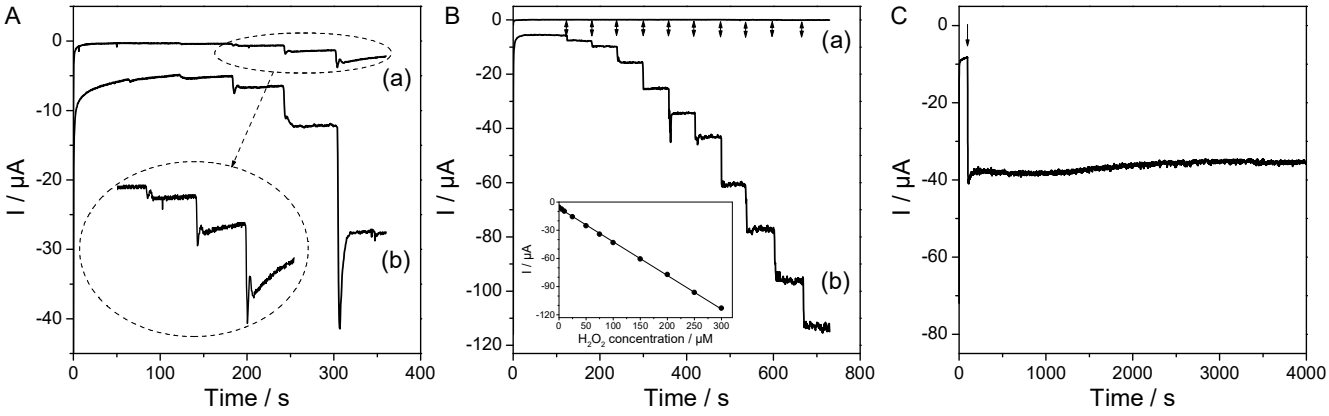

Fig. 6. Amperometric responses recorded at ITO electrodes modified with mesoporous silica films bearing $Fe(Htrz)_3$ to the addition of various concentrations of H_2O_2 (in a stirred aqueous solution of 0.1 M $NaNO_3$); (A) Comparison of responses obtained for increasing H_2O_2 concentrations at applied potentials of respectively (a) -0.2 V and (b) -0.4 V: (B) comparison of (a) bare ITO and (b) the film electrode to additions (arrows) of 5, 10, 25, 50, 75, 100, 150, 200, 250 and 300 µM H_2O_2 (calibration data in inset); (C) Amperometric response to 100 µM H_2O_2 (addition at arrow) recorded for more than one hour.

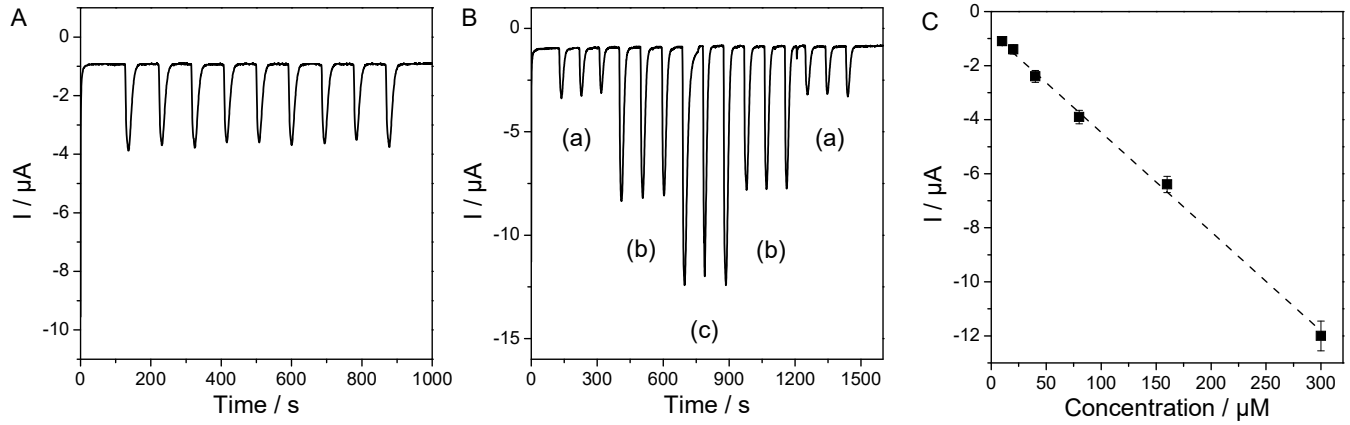

Fig. 7. FIA responses recorded at ITO electrodes modified with mesoporous silica films bearing $Fe(Htrz)_3$ to the injections of 100 µL aliquots of H_2O_2 (in an aqueous carrier solution of 0.1 M $NaNO_3$ flowing at 1 mL min^{-1}); (A) nine successive injections of 30 µM H_2O_2; (B) three successive injections of (a) 30, (b) 150 and (c) 300 µM H_2O_2; (C) Calibration curve.